

INTERPRETING CLIP WITH SPARSE LINEAR CONCEPT EMBEDDINGS (SpLiCE)

Usha Bhalla*
Harvard University ^{a,b}

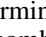
Alex Oesterling*
Harvard University ^b

Suraj Srinivas
Harvard University ^b

Flavio P. Calmon[†]
Harvard University ^b

Himabindu Lakkaraju[†]
Harvard University ^{b,c}

ABSTRACT

CLIP embeddings have demonstrated remarkable performance across a wide range of computer vision tasks. However, these high-dimensional, dense vector representations are not easily interpretable, restricting their usefulness in downstream applications that require transparency. In this work, we empirically show that CLIP’s latent space is highly structured, and consequently that CLIP representations can be decomposed into their underlying semantic components. We leverage this understanding to propose a novel method, Sparse Linear Concept Embeddings (SpLiCE ) , for transforming CLIP representations into sparse linear combinations of human-interpretable concepts. Distinct from previous work, SpLiCE does not require concept labels and can be applied post hoc. Through extensive experimentation with multiple real-world datasets, we validate that the representations output by SpLiCE can explain and even replace traditional dense CLIP representations, maintaining equivalent downstream performance while significantly improving their interpretability. We also demonstrate several use cases of SpLiCE representations including detecting spurious correlations, model editing, and quantifying semantic shifts in datasets. Code is provided at <https://github.com/AI4LIFE-GROUP/SpLiCE>.

tic information in their representations, to help with a wide variety of downstream tasks, such as object classification, scene recognition, or action recognition. However, it is often difficult to enforce explicit encoding of these semantics within model representations, and even harder to interpret these semantics post hoc. Further, these model representations can be brittle, encoding idiosyncratic patterns specific to individual datasets, as opposed to high-level semantic information. Multimodal models have been proposed as a potential solution to this brittleness issue, and methods such as CLIP Radford et al. [2021] have empirically been found to provide highly performant, semantically rich representations of image data. The richness of these representations is evident from their high performance on a wide variety of tasks, such as zero-shot classification and image retrieval Radford et al. [2021], image captioning Mokady et al. [2021], and image generation Ramesh et al. [2022]. However, despite their performance, it remains unclear how to quantify the semantic content contained in their dense representations. In this work, we answer the question: *how can we interpret CLIP embeddings in terms of the semantics of the underlying data they encode?*

Existing machine learning literature in areas such as concept bottleneck models Koh and Liang [2017], disentangled representation learning Bengio [2013], and mechanistic interpretability Olah et al. [2017] have proposed various approaches to understanding the semantics behind representations. However, these methods generally require a predefined set of concepts Kim et al. [2018], data with concept labels Hsu et al. [2023], or rely on qualitative visualizations, which can be unreliable Geirhos et al. [2023]. Similar to these lines of work, we aim to recover representations that reflect the underlying semantics of the inputs. However, distinct from these works, we propose to do this in a post hoc fashion, without concept labels, training, or qualitative analysis of visualizations.

In this work, we leverage the highly structured and multimodal nature of CLIP embeddings for interpretability, and propose SpLiCE, which decomposes CLIP representations into a set of human-interpretable, semantically meaningful concepts. Our overall contributions are:

- In Sections 3 and 4, we formalize the sufficient conditions under which decomposition is feasible, and

1 Introduction

Natural images contain complex semantic information, such as the objects they contain, the scenes they depict, the actions performed, and the relationships between them. Machine learning models on visual data aim to encode this seman-

* Equal contribution, order by coin flip.

† Equal contribution, alphabetic order.

^a Kempner Institute for the Study of Natural & Artificial Intelligence

^b School of Engineering and Applied Sciences

^c Harvard Business School

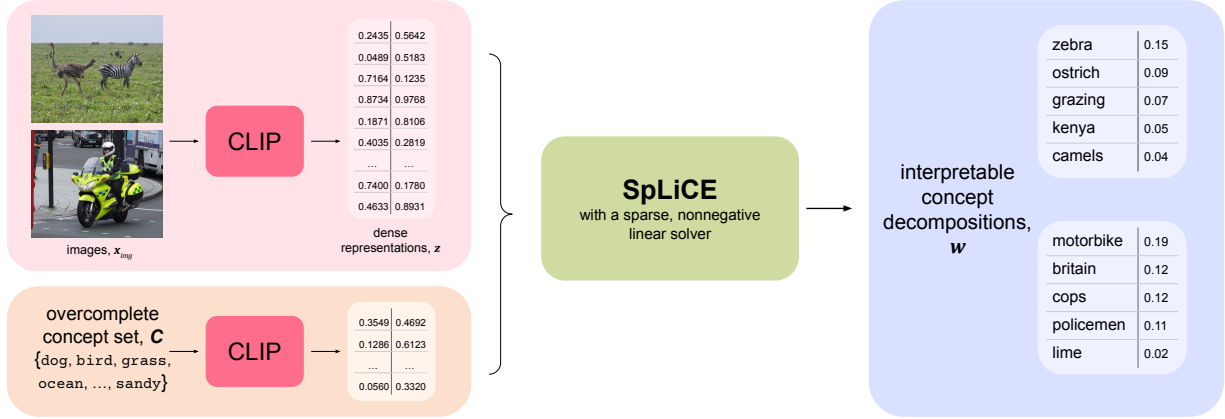


Figure 1: Visualization of SpLiCE, which converts dense, uninterpretable CLIP representations (z) into sparse semantic decompositions (w) by solving for a sparse nonnegative linear combination over an overcomplete concept set (C).

then introduce SpLiCE, a novel method that decomposes dense CLIP embeddings into sparse combinations of human-interpretable, semantic concepts.

- Our extensive experiments in Section 5 reveal that SpLiCE recovers highly sparse¹, interpretable representations with minimal loss in performance on downstream tasks, while accurately capturing the semantics of the underlying inputs.
- In Section 6, we present three case studies for applying SpLiCE: spurious correlation detection, model editing, and quantifying distribution shifts in datasets. We find that SpLiCE is able to uncover unknown biases in datasets, such as the problematic prevalence of women in bikinis in CIFAR100 and the out-of-distribution increase in yellow cars in the early 2000s in the Stanford Cars dataset, while also allowing for intervention on such correlations via representation and model editing.

2 Related Work

Linear Representation Hypothesis. In language modeling, the *linear representation hypothesis* suggests that semantic concepts are organized linearly in the latent space of a model Mikolov et al. [2013], Park et al. [2023], Arora et al. [2018, 2016], Faruqui et al. [2015]. Recent work has also shown that multimodal models behave like bags-of-words, independent of input sequence order Yuksekgonul et al. [2022a]. Merullo et al. [2022] and Seth et al. [2023] show that there exists a linear mapping between image and text embeddings in arbitrary models. Motivated by these findings, we show that the linear representation hypothesis exists in a modality-agnostic semantic space, allowing for a translation between dense, modality-specific embeddings and sparse, semantic representations.

¹we recommend and use sparsity levels of ~ 10 -30 in practice

Concept-based Explanations. Concept Bottleneck Models (CBMs) Koh et al. [2020], and earlier work on attribute based models Lampert et al. [2009], Torresani et al. [2010], Kumar et al. [2009] learn an intermediate representation of scores over concepts for use with a final linear layer, creating interpretable representations that can be intervened on to correct biases and mistakes in models. However, CBMs require training constrained architectures with concept-labeled data, and recent work has shown that CBMs can learn to leak downstream task information through the concept bottleneck layer and may fail to satisfy notions of interpretability and utility Margeloiu et al. [2021], Mahinpei et al. [2021].

Mechanistic Interpretability and Disentanglement. Mechanistic interpretability explains representations through model activations, by labelling circuits and neurons in networks via feature visualization Olah et al. [2017, 2020], or by measuring concept activations and directions in latent space Bau et al. [2017], Fong and Vedaldi [2018], Kim et al. [2018], McGrath et al. [2022], Lucieri et al. [2020], Zhou et al. [2018]. Fel et al. [2023] combine these methods, using dictionary learning to extract visual concept activations, whose semantics can be identified via feature visualization.

Work in disentangled representation learning has developed architectures that capture independent factors of variation in data Hsu et al. [2023], Bricken et al. [2023], Chen et al. [2018], Bengio [2013], Comon [1994], Hyvärinen and Oja [2000], allowing for manual probing of disentangled representations for human-interpretable concepts. While promising, these methods all rely on labelled concept sets, manual labelling of visualizations, or computationally intensive exhaustive searches over networks. Furthermore, Geirhos et al. [2023], Makelov et al. [2023] showcase the unreliability of feature visualization and activation patching, respectively.

CLIP Interpretability. The works most methodologically similar to ours leverage the semantic structure of CLIP and its text encoder to provide explanations. Moayeri et al. [2023], Yuksekgonul et al. [2022b], and Yun et al. [2022]

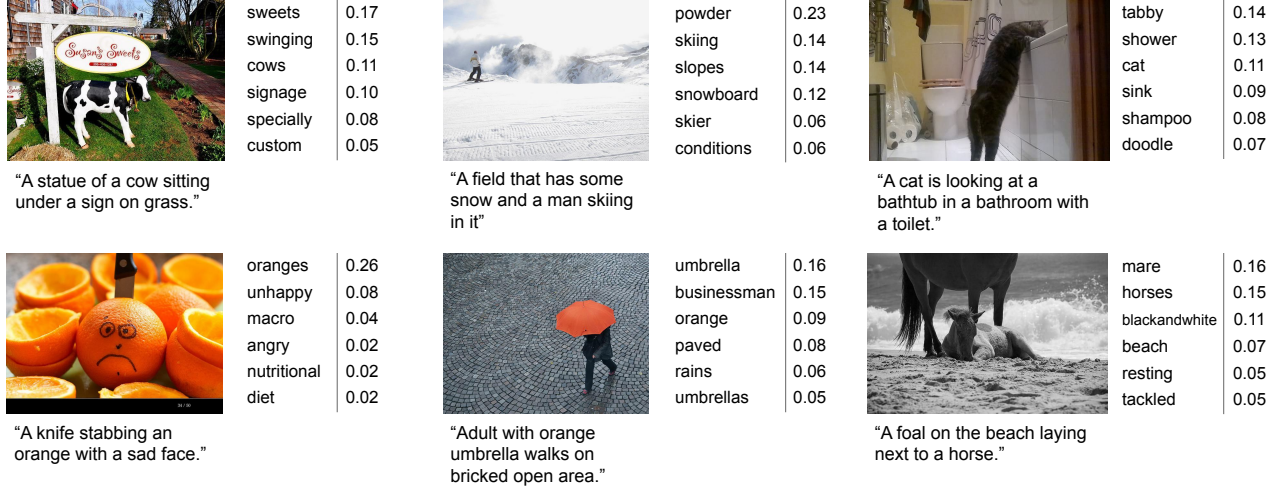


Figure 2: Example images from MSCOCO shown with their captions below and their concept decompositions on the right. We display the top six concepts for visualization purposes, but images in the figure had decompositions with 7-20 concepts.

construct concept similarity scores of image embeddings for use by downstream CBMs or probes, but these scores do not provide semantic decompositions of the original embeddings, and are not interpretable due to their lack of sparsity and nonnegativity. Chen et al. [2023] train a custom vision-language architecture with a sparse latent dictionary, but their method relies on properties of transformer backbones and cannot be used post-hoc to explain existing models. Gandelsman et al. [2023] also leverage the text encoder of CLIP to explain components of the image embedding, but are limited to ViT architectures and take a mechanistic interpretability-style approach requiring a probe dataset of text. Finally, Chattopadhyay et al. [2023] use orthogonal matching pursuit to solve the a similar sparse dictionary learning problem over CLIP image embeddings and text explanation embeddings, but do not impose non-negativity and use complex explanations that do not capture the individual semantic units making up an image.

3 When do Sparse Decompositions Exist?

In this section, we aim to answer the question: *under what conditions can CLIP representations be decomposed into sparse semantic representations?* To address this question, we are required to reason about both the properties of CLIP as well as the properties of the underlying data.

Notation. Let $\mathbf{x}^{\text{img}} \in \mathbb{R}^{d_i}$, $\mathbf{x}^{\text{txt}} \in \mathbb{R}^{d_t}$ be image and text data respectively. Given CLIP image encoder $f : \mathbb{R}^{d_i} \rightarrow \mathbb{R}^d$ and text encoder $g : \mathbb{R}^{d_t} \rightarrow \mathbb{R}^d$, we define CLIP representations in \mathbb{R}^d as $\mathbf{z}^{\text{img}} = f(\mathbf{x}^{\text{img}})$ and $g(\mathbf{x}^{\text{txt}}) = \mathbf{z}^{\text{txt}}$. Our method uses dictionary learning to approximate \mathbf{z}^{img} with a concept decomposition $\mathbf{w}^* \in \mathbb{R}_+^c$ over a fixed concept vo-

cabulary $\mathbf{C} \in \mathbb{R}^{d \times c}$. We define the resulting reconstruction of \mathbf{z}^{img} from \mathbf{C} and \mathbf{w}^* as $\hat{\mathbf{z}}^{\text{img}}$.

The overall goal of our method is to approximate $f(\mathbf{x}^{\text{img}}) \approx \mathbf{C}\mathbf{w}^*$, such that \mathbf{w}^* is non-negative and sparse, and in this section we formalize when this is possible. We begin by considering a data-generating process for coupled image and text samples. Specifically, we model the generative process parameterized by a k -dimensional latent concept vector $\omega \in \mathbb{R}_+^{k_1}$ and a random vector $\epsilon \in \mathbb{R}^{k_2}$ as

$$\begin{aligned} \mathbf{x}^{\text{img}} &= h^{\text{img}}(\omega, \epsilon), \quad \mathbf{x}^{\text{txt}} = h^{\text{txt}}(\omega, \epsilon), \\ \omega &\sim \rho, \\ \epsilon &\sim \phi, \end{aligned}$$

where ρ is a prior distribution over semantic concepts, ϕ is a prior distribution over nonsemantic concepts (such as camera orientation and lighting for images or sentence structure for text), and $h^{\text{img}} : \mathbb{R}^{k_1+k_2} \rightarrow \mathbb{R}^{d_i}$, and $h^{\text{txt}} : \mathbb{R}^{k_1+k_2} \rightarrow \mathbb{R}^{d_t}$ are mappings from latent variables (ω, ϵ) to data. In addition, we assume unique invertibility, i.e., for every \mathbf{x}^{img} , \mathbf{x}^{txt} , there exists a unique pre-images (ω, ϵ) that generated it. Here, each coordinate $\omega_i \in \mathbb{R}_+$ encodes the degree of prevalence of the i^{th} concept in the underlying data, where a concept is a semantic piece of information that can be described in a single English word. Under this generative model, a total of k_1 distinct concepts can be encoded by inputs, one corresponding to each coordinate of ω .

Note that these data-generating processes and latent concept vectors cannot be directly observed. We now identify a key property, the sparsity of data in concept space.

Property 3.1. Data is sparse in concept space. In other words, for some $\alpha \ll k_1$, we have $\|\omega\|_0 \leq \alpha, \forall \omega \sim \rho$.

The next property is the most critical one and posits that CLIP models are linear over concepts, which is also closely related to the linear representation hypothesis Park et al. [2023]. In addition, we posit that CLIP is largely invariant to

the ‘non-semantic’ factors ϵ in the image. For example, the embedding of a cat photographed from two angles should be the same. To formalize this in our context, recall that the image and text encoders of CLIP are given by f and g , respectively.

Now consider $f(\mathbf{x}^{\text{img}}) = f(h^{\text{img}}(\omega, \epsilon)) \triangleq (f \circ h^{\text{img}})(\omega, \epsilon)$, and similarly $g(\mathbf{x}^{\text{txt}}) = (g \circ h^{\text{txt}})(\omega, \epsilon)$. Note that while these composition maps $f \circ h^{\text{img}}$ and $g \circ h^{\text{txt}}$ can be nonlinear in general, the following property indicates that these are in fact linear functions of ω , and independent of ϵ .

Property 3.2. CLIP encoders are (1) independent of ϵ , i.e.,

$$\begin{aligned} g \circ h^{\text{img}}(\omega) &\triangleq g \circ h^{\text{img}}(\omega, \epsilon), \\ g \circ h^{\text{txt}}(\omega) &\triangleq g \circ h^{\text{txt}}(\omega, \epsilon), \end{aligned}$$

and (2) linear in concept space ω , i.e., $g \circ h^{\text{txt}}$ and $f \circ h^{\text{img}}$ are linear wrt ω .

Note that this assumption does not require f, g to be linear, rather it requires its composition with the underlying generative model $h^{\text{img}}, h^{\text{txt}}$ to result in a linear map. This implies that the CLIP encoders f, g perform an ‘inversion’ of the latent generative process, up to a linear transformation. This assumption falls in line with the idea that computer vision systems must behave like ‘inverse graphics’ models Hinton [2013], Romaszko et al. [2017]. In Appendix E.1, we provide evidence for such linearity of CLIP in a toy setting.

We now make another assumption connecting the image and text representations of CLIP, requiring them to be equal. This is approximately enforced by CLIP’s training objective, which requires image and text representations to align.

Property 3.3. For the same latent concept vector ω , the CLIP image and text representations are equal to each other, i.e., $f \circ h^{\text{img}}(\omega) = g \circ h^{\text{txt}}(\omega)$.

Our final assumption involves the computation of the basis vectors in concept space. These are given by $\mathbf{e}_i \in \mathbb{R}^k$, which are unique one-hot vectors with a one at the i^{th} coordinate. Consider the mapping of these ‘basis’ concepts in text space. As concepts can be described by a single English word without any grammatical structure or phrasing involved, the mapping of a basis vector to text is independent of non-semantic noise. The following assumption states that these are text strings of individual words depicting that concept.

Property 3.4. Basis concepts \mathbf{e}_i map to individual words in text space, i.e., $h^{\text{txt}}(\mathbf{e}_i, \epsilon) = h^{\text{txt}}(\mathbf{e}_i)$ is a text string of an individual word representing that concept.

Under this assumption, if coordinate i corresponds to the concept cat, then $h^{\text{txt}}(\mathbf{e}_i) = \text{"cat"}$. Now consider the encoding of these ‘basis’ concepts in text space, i.e., $\mathbf{c}_i^{\text{txt}} = (g \circ h^{\text{txt}})(\mathbf{e}_i)$. Let us also define the concept dictionary $\mathbf{C} = [\mathbf{c}_0^{\text{txt}}; \mathbf{c}_1^{\text{txt}}; \dots; \mathbf{c}_k^{\text{txt}}] \in \mathbb{R}^{d \times k_1}$ as a matrix of the text concept bases. Thus the concept dictionary \mathbf{C} can be equivalently represented as a sequence of words, e.g.: [cat, ocean, sky, ...], encoding these concepts in text space. Given these assumptions, we can write the following statement about CLIP representations.

Theorem 3.5. Given Properties 4.1 - 4.4, CLIP image embeddings f can be written as a sparse linear combination of text embeddings, i.e.,

$$f(\mathbf{x}^{\text{img}}) = \mathbf{C}\mathbf{w}; \quad \text{s.t.} \quad \|\mathbf{w}\|_0 \leq \alpha$$

where $\mathbf{w} \in \mathbb{R}_+^{k_1}$, and $\mathbf{C} \in \mathbb{R}^{d \times k_1}$, which is the concept dictionary obtained from word embeddings of individual words, as described above.

Proof Sketch. Property 3.1 + 3.2 together show that f can be written as a sparse linear combination of image embeddings, and Property 3.3 + 3.4 help transfer this result to the text embeddings of individual words. We provide the full proof in Appendix C. \square

Thus we have shown that given natural assumptions about CLIP and the data generating process in terms of Properties 3.1–3.4, CLIP models have a sparse decomposition property. The critical idea here is Property 3.2, which requires models to behave linearly in concept space. In the next section, we propose a method to perform this sparse decomposition.

4 Method

In this section we introduce SpLiCE, a method for expressing CLIP’s image representations as sparse, nonnegative, linear combinations of a concept dictionary. In the subsections that follow, we outline our design choices, including how we choose the concept dictionary in Section 4.1, how we bridge the modality gap between CLIP’s images and text representations in Section 4.2, and our method for decomposition in Section 4.3.

4.1 Concept Vocabulary

Natural language is an intuitive, interpretable, and compact medium for communicating semantic information. Thus, we choose to represent the semantic content contained in CLIP embeddings as combinations of semantic concepts expressed in natural language. We formalize this as dictionary learning problem over a concept vocabulary of natural language embeddings, where we define concepts as a semantic visual unit that can be expressed by a single English word.

Previous works have found that existing concept-based explanation methods are highly sensitive to the concept vocabulary chosen Ramaswamy et al. [2022], and a prevalent critique of methods like traditional Concept Bottleneck Models is that they rely on a well-specified and expert-chosen concept set for the task at hand. Furthermore, there often exists a direct trade-off between the size of the concept set and the interpretability offered by the method, as an explanation with too many concepts fails to be comprehensible to humans Ramaswamy et al. [2022]. However, because we enforce sparsity in our concept decompositions, we can choose to have a large, overcomplete vocabulary that well spans the

concept space of CLIP and thus is expert- and task-agnostic. To construct our vocabulary, we consider all one-word English tokens in the text captions of the LAION-400m dataset Schuhmann et al. [2021]. We filter the captions to remove any NSFW samples and choose the top 10000 most common words to be our concept vocabulary.

4.2 Modality Alignment

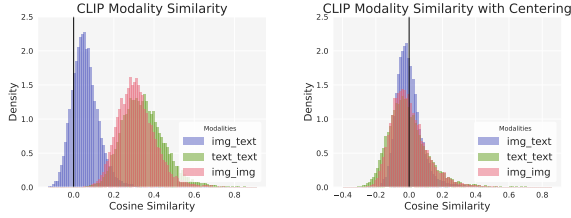


Figure 3: Average cosine similarity across pairs of image-text, image-image, and text-text data from MSCOCO. After aligning modalities, the distribution of similarities is centered around zero.

In order to decompose images into text concepts, we must ensure that the representations of images span those of our concept set. However, Liang et al. [2022] show the existence of a modality gap in CLIP, where image and text embeddings can lie in non-overlapping spaces on the unit sphere. Empirically, we find that CLIP image and text embeddings exist on two cones, as the distribution of pairwise cosine similarities between MSCOCO image and text embeddings concentrate at a positive value (Fig. 3). To rectify this, we mean-center CLIP images with the image cone mean, estimated over MSCOCO (μ_{img}), and compute decompositions over the mean-centered concept vocabulary (μ_{con}). Note that the embeddings need to be re-normalized after centering to ensure they lie on the unit-sphere. If we wish to convert our decompositions back into dense representations ($\hat{\mathbf{z}}^{\text{img}}$), we uncenter the normalized dense embeddings $\hat{\mathbf{z}}^{\text{img}}$ by adding the image mean back in and normalizing once again, to ensure they lie on the same cone as the original CLIP embeddings (\mathbf{z}^{img}).

4.3 Sparse Nonnegative Concept Decomposition

We consider two desiderata when semantically decomposing dense CLIP representations: *sparsity*, and *nonnegativity*. A large body of work has shown that sparsity and nonnegativity yield greater interpretability in representations, as sparse sets can be comprehended all at once, while negative semantics remain unintuitive and difficult to conceptualize. Ramaswamy et al. [2022], Faruqui et al. [2015], ACichocki et al. [2009], Murphy et al. [2012], Fyshe et al. [2014, 2015], Lipton [2017], Ribeiro et al. [2016].

This motivates our optimization problem: reconstruct a CLIP image embedding with a *sparse, nonnegative* com-

bination of concepts. Let $\sigma(x) = x/\|x\|_2$ be the normalization operation. Given a set of concept vocabulary $\mathbf{x}^{\text{con}} = [\text{"dog"}, \text{"bird"}, \text{"grass"}, \dots]$, our centered concept dictionary

$$\mathbf{C} = [\sigma(g(\mathbf{x}_1^{\text{con}}) - \mu_{\text{con}}), \dots, \sigma(g(\mathbf{x}_c^{\text{con}}) - \mu_{\text{con}})],$$

and a centered CLIP image embedding

$$\mathbf{z} = \sigma(\mathbf{z}^{\text{img}} - \mu_{\text{img}}),$$

we seek to find the sparsest solution that gives us a cosine similarity score of at least $1 - \epsilon$ for some small ϵ :

$$\min_{\mathbf{w} \in \mathbb{R}_+^c} \|\mathbf{w}\|_0 \quad \text{s.t.} \quad \langle \mathbf{z}, \sigma(\mathbf{C}\mathbf{w}) \rangle \geq 1 - \epsilon. \quad (1)$$

As is standard practice, we relax the ℓ_0 constraint and reformulate this as a minimization of MSE with an ℓ_1 penalty, to construct the following convex relaxation² of Eq. (1):

$$\min_{\mathbf{w} \in \mathbb{R}_+^c} \|\mathbf{C}\mathbf{w} - \mathbf{z}\|_2^2 + 2\lambda\|\mathbf{w}\|_1. \quad (2)$$

Note that the linearity of \mathbf{w} allows us to interpret the magnitude of a coordinate w_i as the prominence of concept i in the image \mathbf{x}^{img} . With the solution to our optimization problem defined as \mathbf{w}^* , our reconstructed embedding is then

$$\hat{\mathbf{z}}^{\text{img}} = \sigma(\mathbf{C}\mathbf{w}^* + \mu_{\text{img}}). \quad (3)$$

5 Experiments

In this section we evaluate our method to ensure that the added interpretability results in minimal loss in performance for downstream tasks and accurately reflects the semantic content of representations.

5.1 Setup

Models. All experiments shown in the main paper are done with the OpenCLIP ViT-B/32 model Ilharco et al. [2021] with results for an additional model in Appendix 13. For all zero-shot classification tasks we use the prompt template “A photo of a { }”. **Datasets.** We use CIFAR100 Krizhevsky et al. [2009], MIT States Isola et al. [2015], CelebA Liu et al. [2015], MSCOCO Lin et al. [2014], and ImageNetVal Deng et al. [2009] for our experiments.

Decomposition. For all experiments involving concept decomposition, we use sklearn’s Pedregosa et al. [2011] Lasso solver with a non-negativity flag and an ℓ_1 penalty that results in solutions with l_0 norms of 15-30 (around 0.2 for most datasets), unless stated otherwise, in accordance with the threshold of 32 concepts found by Ramaswamy et al. [2022]. We use a concept vocabulary chosen from a subset of LAION tokens as described in Section 4.1. Both images and concepts are centered as mentioned in Section 4.2, with the image mean used for centering computed over the MSCOCO train set and the concept mean computed over our chosen vocabulary.

²For more discussion on the relationship between Eq. (1) and Eq. (2), see Appendix, Sec. A

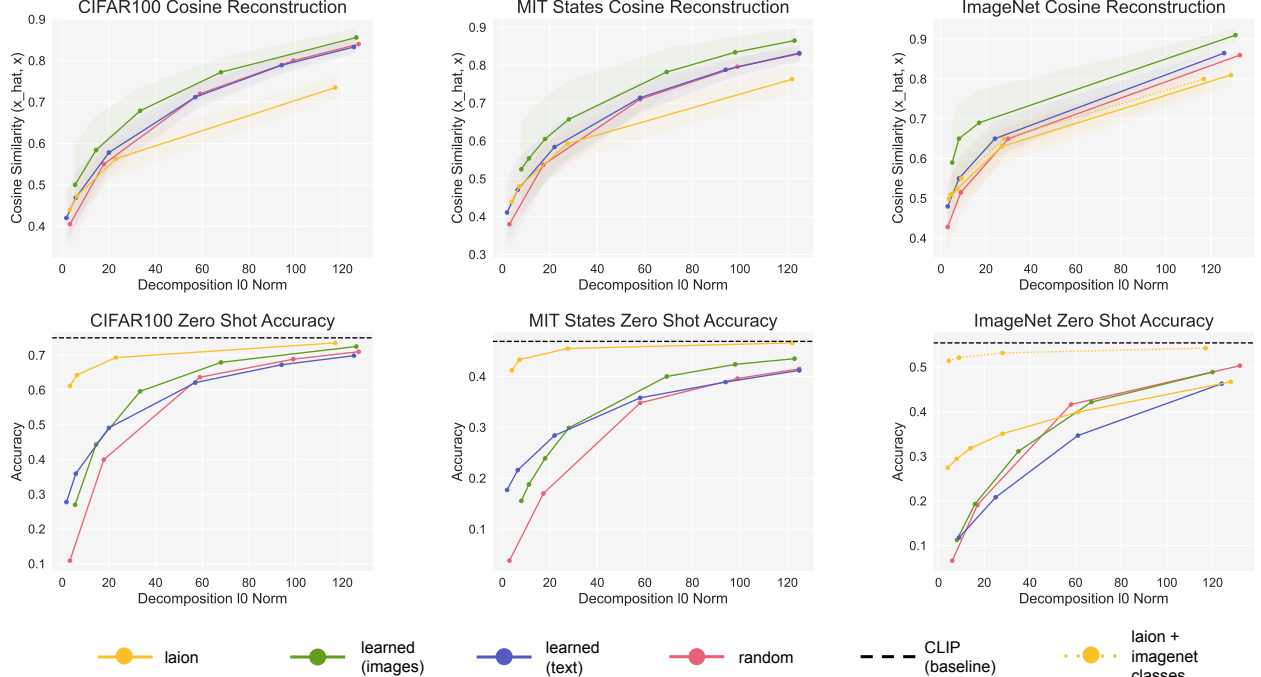


Figure 4: Performance of SpLiCE decomposition representations on zero-shot classification tasks (bottom row) and cosine similarity between CLIP embeddings and SpLiCE embeddings (top row). We find that the semantic dictionary collected from LAION (yellow) performs the best for zero-shot classification tasks, but that the dictionary learned over images (green) is best for reconstructing embeddings with minimal cosine error.

5.2 Sparsity-Performance Tradeoffs

We assess the performance of SpLiCE decompositions by evaluating the reconstruction error between SpLiCE representations and CLIP embeddings, the zero-shot performance of SpLiCE, and the retrieval performance of the various embeddings. We compare the performance of decompositions generated from our semantic concept vocabulary to decompositions over a random vocabulary and dictionary learned vocabularies. All vocabularies include 10,000 concepts, where the random vocabulary is sampled from a Gaussian distribution and normalized to lie on a hypersphere. The learned vocabularies are generated by using the Fast Iterative Shrinkage-Thresholding Algorithm (FISTA) Beck and Teboulle [2009] to learn the optimal dictionary over either the MSCOCO image corpus or caption corpus.

In Figure 4, we visualize the cosine reconstruction and zero-shot accuracy of image decompositions with various dictionaries. We find that while our semantic concept dictionary does not reconstruct samples as well as the learned dictionaries with regard to cosine similarity, it significantly outperforms the decompositions with random and learned dictionaries for zero-shot classification tasks. In particular, decompositions with low sparsity (<5 nonzero concepts) still provide enough semantic information to classify CIFAR100 and MIT States images with similar performance to the vanilla CLIP embeddings. We note that performance on ImageNet is worse than the other datasets because many ImageNet classes are animal species that cannot easily be described by a few single-word semantic concepts (e.g. ‘boston

bull’). Adding these class labels to our concept dictionary increases performance significantly, as shown by the dotted yellow line in Figure 4. We note that interestingly, concept dictionaries learned over images outperform dictionaries learned over text for cosine reconstruction, but the opposite is true for zero-shot performance at high sparsities. We evaluate probing performance in the Appendix (Tables 3, 4).

We finally test the performance of SpLiCE embeddings on text-to-image and image-to-text retrieval tasks. We evaluate retrieval over various 1024 sample subsets of MSCOCO, and assess recall performance for the top- k closest embeddings of the opposite modality. We visualize $k = \{5\}$ for text-to-image retrieval in Figure 5, with $k = \{1, 10\}$ and image-to-text in the Appendix (Figure 12). We note that while the decompositions do not perfectly match the performance of dense CLIP embeddings at high sparsities, an order of magnitude reduction in memory (l_0 norm ≈ 50) only leads to a drop in recall of about 15%.

5.3 Concept Based Explanations of Images

We qualitatively evaluate SpLiCE decompositions as measures of the semantic content of the images they represent. In Figure 2 we provide six sample decompositions from MSCOCO with their corresponding captions. We display the top six concepts for each image, and find that they generally well-describe the semantics of the images. As such, we propose that these decompositions can be used as im-

age taggers, or simply as concept-based explanations of the semantic content of CLIP embeddings when used in downstream tasks such as classification.

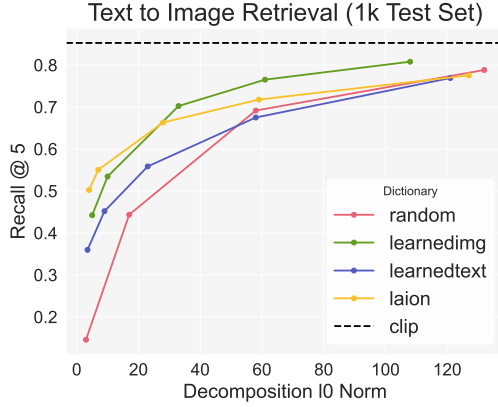


Figure 5: Performance of SpLiCE representations for text-to-image retrieval on MSCOCO.

5.4 Concept Based Explanations of Classes or Datasets

While concept decompositions can be highly useful for explaining the predictions and decisions of any systems relying on CLIP embeddings, we also propose that this method can be used to better understand and summarize datasets. By decomposing entire classes or whole datasets, we can find the underlying semantic distribution of the data. We visualize the top 7 most common concepts in three ImageNet classes ('Bakery', 'Balloon', 'Indian elephant', and 'African elephant') in Figure 6. These decompositions yielded interesting insights into the classes themselves; the second most common concept in the 'Bakery' class was "cupcake," and we indeed found that 7/50 photos in the test class were close-up photos of cupcakes. The 'Balloon' class does not feature blow up party balloons, but rather hot-air balloons, as indicated by the concepts "parachute" and "flying". For the two elephant classes, we see that the decompositions contain information about the backgrounds, such as "jungle", "kerala", and "africa", thus encoding the nuances between the two species.

6 Case Studies and Applications of SpLiCE

In this section, we present three case studies using SpLiCE: (1) spurious correlation and bias detection in datasets 6.1, (2) debiasing classification models 6.2, and (3) monitoring distribution shift 6.3.

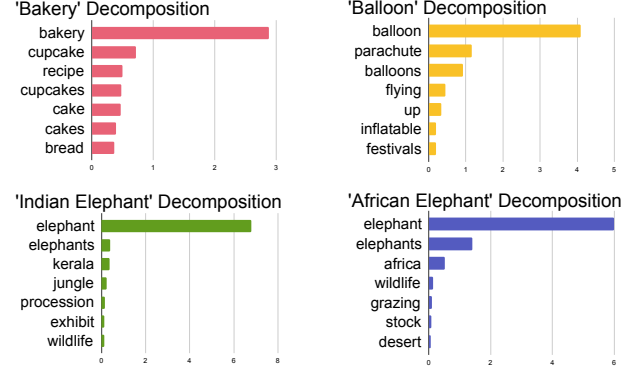


Figure 6: SpLiCE decompositions of ImageNet 'Bakery', 'Balloon', 'Indian Elephant', 'African Elephant' classes.

6.1 Case Study: Spurious Correlation Detection

A key motivating application for SpLiCE is the ability to automatically summarize datasets semantically. We find that this is particularly helpful for auditing bias or spurious correlations in datasets, which would otherwise require labels of both the subgroup and the spuriously correlated feature. We present a case study of the two adult classes of CIFAR100: 'man' and 'woman'. Upon decomposing these classes, we found that "bra" and "swimwear" were two of the top ten most common concepts in the 'woman' class. On the other hand, the only clothing-related concepts that appear in the top 50 most activated concepts for 'men' are {"uniform", "tuxedo", "apparel"}. We visualize a histogram of the concept weights on swimwear and undergarment related concepts {"swimwear", "bra", "trunks", "underwear"} in Figure 7 across both the train and test sets, and find that these concepts are much more likely to be activated for women than men. This phenomenon was confirmed via manual inspection of the CIFAR100 dataset, where at least 8 of the 100 images in the 'woman' test class feature women in bikinis, revealing stereotype bias in this popular dataset.

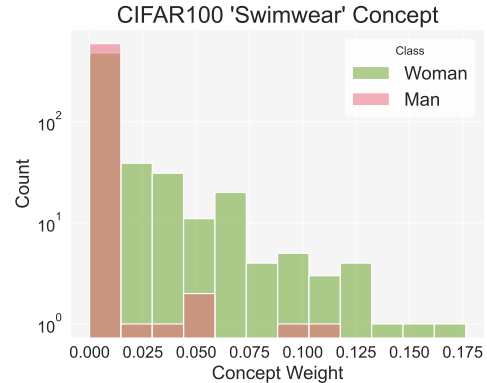


Figure 7: Distribution of "Swimwear" concept in 'Woman' and 'Man' classes of CIFAR100.

6.2 Case Study: Model Editing

Another key application of concept decompositions is using them to isolate specific information, allowing for fine-grained intervention. This intervention can be performed on the embeddings themselves, where we can zero out a concept and reconstruct the input without that information, or probes built upon the decompositions, where we can manually alter the relationships between concepts and class labels (similar to a concept bottleneck Koh et al. [2020]).

Consider a facial recognition classifier trained on images of CelebA. We wish for this classifier to be invariant to the presence of glasses, but we are unsure if there exist spurious correlations between certain individuals and the presence of eyewear. We thus wish to remove the concept of “eyewear” or “glasses” from the image representations, such that they cannot be leveraged for downstream classification. We can do so by simply zero-ing out any weight placed upon those concepts in our SpLiCE decompositions, and evaluate if a zero-shot classifier can detect the presence of glasses. We report performance of zero-shot classifier in identifying the concept “glasses” before and after intervention in rows ‘ZS SpLiCE’ and ‘Intervention SpLiCE’ respectively. Vanilla CLIP performance is given as a baseline in ‘ZS CLIP’. We see that removing that intervention reduces accuracy of the zero-shot classifier from 0.88 to 0.69 (where 0.50 is random). We also evaluate intervention on linear probes, where we ablate probe weights of the concept, and see that the glasses probe’s accuracy drops from 0.88 to 0.59 after invention. We provide gender classification performance for the same as a proxy for facial recognition, and see that intervention on “glasses” for both zero-shot and probing tasks has minimal effect on gender classification.

Table 1: Evaluation of Intervention on the Concept ‘Glasses’

	GENDER	GLASSES
ZS CLIP	0.98	0.91
ZS SpLiCE	0.97	0.88
INTERVENTION SpLiCE	0.96	0.69
LINEAR PROBE	0.89	0.88
INTERVENTION PROBE	0.85	0.59

6.3 Case Study: Distribution Shift Monitoring

We present a final case study using SpLiCE to monitor distribution shift. This can help identify differences between training and inference distributions or evaluate how a continually sampled dataset changes over time. In this experiment we consider the Stanford Cars dataset, which contains photos of cars from 1991 to 2012, including their make and year labels. By decomposing photos of cars from each year, we can view how the distribution changed yearly. We visualize the weights of the concepts “convertible” and “yellow”

from our decompositions, as well as the actual percentage of cars from each year that were convertibles or yellow in Figure 8. Note the right-hand y-axis, corresponding to the weight of the given concept c_i , does not have a meaningful unit of measure or scale. We find that the trends in the groundtruth concept prevalence generally closely match that of the predicted/decomposed concepts, allowing us to visualize which years convertibles or yellow cars were popular or out-of-distribution with respect to other years.

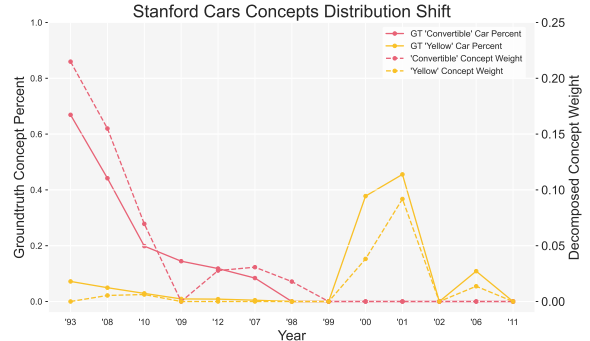


Figure 8: Visualization of the presence of convertibles (pink lines) and yellow cars (yellow lines) in Stanford Cars over time. SpLiCE concept weights (dotted) closely track the groundtruth concept prevalence (solid) for both concepts.

7 Discussion

In this work, we show that the information contained in CLIP embeddings can be approximated by a linear combination of simple semantic concepts, allowing us to interpret representations with sparse, nonnegative dictionary learning. We propose SpLiCE, a method to transform the dense, uninterpretable embeddings of CLIP into human-interpretable sparse concept decompositions.

We empirically demonstrate that the improved interpretability of SpLiCE does not come at a cost to downstream performance, and provide three concrete use cases for SpLiCE: spurious correlation detection, model intervention and editing, and distribution shift monitoring, showcasing the benefits of using interpretable embeddings with known semantic content. We highlight that SpLiCE embeddings do not need to be used as a replacement for dense CLIP embeddings, but can also serve as a post-hoc interpretation of them.

Limitations. In this work, we only consider one word English concepts for our concept vocabulary; however, there exist many concepts that cannot be described under those constraints, such as “butter chicken”. In addition, we only consider linear decompositions, due to its convexity and potential added interpretability. Future work may consider using nonlinear decomposition solvers to achieve more

accurate decompositions. SpLiCE also uses an ℓ_1 penalty as the relaxation for ℓ_0 regularization, but future work may consider alternative relaxations or even binary concept weights.

Broader Impact.

Similar to many works in the field of interpretability, our work provides greater understanding of the behavior of models, including but not limited to the broader implicit biases they perpetuate as well as mistakes made on individual samples. We believe this is particularly salient for CLIP, which is used in a variety of applications that are widely used. We hope that insights gained from such interpretability allow users to make more informed decisions regarding how they interact with and use CLIP, regardless of their familiarity with machine learning or domain expertise in the task they are using CLIP for. We also highlight that SpLiCE can be used as a visualization-like tool for exploring and summarizing datasets at scale, allowing for easier auditing of spurious correlations and biases in both datasets and models.

Acknowledgements and Disclosure of Funding

This work is supported in part by the NSF awards IIS-2008461, IIS-2040989, IIS-2238714, FAI-2040880, and research awards from Google, JP Morgan, Amazon, Adobe, Harvard Data Science Initiative, and the Digital, Data, and Design (D³) Institute at Harvard. AO is supported by the National Science Foundation Graduate Research Fellowship under Grant No. DGE-2140743, and UB is funded by the Kempner Institute Graduate Research Fellowship. The views expressed here are those of the authors and do not reflect the official policy or position of the funding agencies.

References

- Alec Radford, Jong Wook Kim, Chris Hallacy, Aditya Ramesh, Gabriel Goh, Sandhini Agarwal, Girish Sastry, Amanda Askell, Pamela Mishkin, Jack Clark, Gretchen Krueger, and Ilya Sutskever. Learning transferable visual models from natural language supervision. In Marina Meila and Tong Zhang, editors, *Proceedings of the 38th International Conference on Machine Learning*, volume 139 of *Proceedings of Machine Learning Research*, pages 8748–8763. PMLR, 18–24 Jul 2021.
- Ron Mokady, Amir Hertz, and Amit H Bermano. Clip-cap: Clip prefix for image captioning. *arXiv preprint arXiv:2111.09734*, 2021.
- Aditya Ramesh, Prafulla Dhariwal, Alex Nichol, Casey Chu, and Mark Chen. Hierarchical text-conditional image generation with clip latents. *arXiv preprint arXiv:2204.06125*, 1(2):3, 2022.
- Pang Wei Koh and Percy Liang. Understanding black-box predictions via influence functions. In *International conference on machine learning*, pages 1885–1894. PMLR, 2017.
- Yoshua Bengio. Deep learning of representations: Looking forward. In *International conference on statistical language and speech processing*, pages 1–37. Springer, 2013.
- Chris Olah, Alexander Mordvintsev, and Ludwig Schubert. Feature visualization. *Distill*, 2(11):e7, 2017.
- Been Kim, Martin Wattenberg, Justin Gilmer, Carrie Cai, James Wexler, Fernanda Viegas, et al. Interpretability beyond feature attribution: Quantitative testing with concept activation vectors (tcav). In *International conference on machine learning*, pages 2668–2677. PMLR, 2018.
- Kyle Hsu, Will Dorrell, James CR Whittington, Jiajun Wu, and Chelsea Finn. Disentanglement via latent quantization. *arXiv preprint arXiv:2305.18378*, 2023.
- Robert Geirhos, Roland S Zimmermann, Blair Bilodeau, Wieland Brendel, and Been Kim. Don’t trust your eyes: on the (un) reliability of feature visualizations. *arXiv preprint arXiv:2306.04719*, 2023.
- Tomáš Mikolov, Wen-tau Yih, and Geoffrey Zweig. Linguistic regularities in continuous space word representations. In *Proceedings of the 2013 conference of the north american chapter of the association for computational linguistics: Human language technologies*, pages 746–751, 2013.
- Kiho Park, Yo Joong Choe, and Victor Veitch. The linear representation hypothesis and the geometry of large language models. *arXiv preprint arXiv:2311.03658*, 2023.
- Sanjeev Arora, Yuanzhi Li, Yingyu Liang, Tengyu Ma, and Andrej Risteski. Linear algebraic structure of word senses, with applications to polysemy. *Transactions of the Association for Computational Linguistics*, 6:483–495, 2018.
- Sanjeev Arora, Yuanzhi Li, Yingyu Liang, Tengyu Ma, and Andrej Risteski. A latent variable model approach to pmi-based word embeddings. *Transactions of the Association for Computational Linguistics*, 4:385–399, 2016.
- Manaal Faruqui, Yulia Tsvetkov, Dani Yogatama, Chris Dyer, and Noah Smith. Sparse overcomplete word vector representations. *arXiv preprint arXiv:1506.02004*, 2015.
- Mert Yuksekgonul, Federico Bianchi, Pratyusha Kalluri, Dan Jurafsky, and James Zou. When and why vision-language models behave like bags-of-words, and what to do about it? In *The Eleventh International Conference on Learning Representations*, 2022a.
- Jack Merullo, Louis Castricato, Carsten Eickhoff, and Ellie Pavlick. Linearly mapping from image to text space. *arXiv preprint arXiv:2209.15162*, 2022.
- Ashish Seth, Mayur Hemani, and Chirag Agarwal. Dear: Debiasing vision-language models with additive residuals. In *Proceedings of the IEEE/CVF Conference on Computer Vision and Pattern Recognition*, pages 6820–6829, 2023.

- Pang Wei Koh, Thao Nguyen, Yew Siang Tang, Stephen Mussmann, Emma Pierson, Been Kim, and Percy Liang. Concept bottleneck models. In *International conference on machine learning*, pages 5338–5348. PMLR, 2020.
- Christoph H Lampert, Hannes Nickisch, and Stefan Harmeling. Learning to detect unseen object classes by between-class attribute transfer. In *2009 IEEE conference on computer vision and pattern recognition*, pages 951–958. IEEE, 2009.
- Lorenzo Torresani, Martin Szummer, and Andrew Fitzgibbon. Efficient object category recognition using classemes. In *Computer Vision—ECCV 2010: 11th European Conference on Computer Vision, Heraklion, Crete, Greece, September 5–11, 2010, Proceedings, Part I 11*, pages 776–789. Springer, 2010.
- Neeraj Kumar, Alexander C Berg, Peter N Belhumeur, and Shree K Nayar. Attribute and simile classifiers for face verification. In *2009 IEEE 12th international conference on computer vision*, pages 365–372. IEEE, 2009.
- Andrei Margeloiu, Matthew Ashman, Umang Bhatt, Yanzhi Chen, Mateja Jamnik, and Adrian Weller. Do concept bottleneck models learn as intended? *arXiv preprint arXiv:2105.04289*, 2021.
- Anita Mahinpei, Justin Clark, Isaac Lage, Finale Doshi-Velez, and Weiwei Pan. Promises and pitfalls of black-box concept learning models. *arXiv preprint arXiv:2106.13314*, 2021.
- Chris Olah, Nick Cammarata, Ludwig Schubert, Gabriel Goh, Michael Petrov, and Shan Carter. Zoom in: An introduction to circuits. *Distill*, 5(3):e00024–001, 2020.
- David Bau, Bolei Zhou, Aditya Khosla, Aude Oliva, and Antonio Torralba. Network dissection: Quantifying interpretability of deep visual representations. In *Proceedings of the IEEE conference on computer vision and pattern recognition*, pages 6541–6549, 2017.
- Ruth Fong and Andrea Vedaldi. Net2vec: Quantifying and explaining how concepts are encoded by filters in deep neural networks. In *Proceedings of the IEEE conference on computer vision and pattern recognition*, pages 8730–8738, 2018.
- Thomas McGrath, Andrei Kapishnikov, Nenad Tomašev, Adam Pearce, Martin Wattenberg, Demis Hassabis, Been Kim, Ulrich Paquet, and Vladimir Kramnik. Acquisition of chess knowledge in alphazero. *Proceedings of the National Academy of Sciences*, 119(47):e2206625119, 2022.
- Adriano Lucieri, Muhammad Naseer Bajwa, Stephan Alexander Braun, Muhammad Imran Malik, Andreas Dengel, and Sheraz Ahmed. On interpretability of deep learning based skin lesion classifiers using concept activation vectors. In *2020 international joint conference on neural networks (IJCNN)*, pages 1–10. IEEE, 2020.
- Bolei Zhou, Yiyu Sun, David Bau, and Antonio Torralba. Interpretable basis decomposition for visual explanation. In *Proceedings of the European Conference on Computer Vision (ECCV)*, pages 119–134, 2018.
- Thomas Fel, Victor Boutin, Mazda Moayeri, Rémi Cadène, Louis Bethune, Mathieu Chalvidal, Thomas Serre, et al. A holistic approach to unifying automatic concept extraction and concept importance estimation. *arXiv preprint arXiv:2306.07304*, 2023.
- Trenton Bricken, Adly Templeton, Joshua Batson, Brian Chen, Adam Jermy, Tom Conerly, Nick Turner, Cem Anil, Carson Denison, Amanda Askell, et al. Towards monosemanticity: Decomposing language models with dictionary learning. *Transformer Circuits Thread*, page 2, 2023.
- Ricky TQ Chen, Xuechen Li, Roger B Grosse, and David K Duvenaud. Isolating sources of disentanglement in variational autoencoders. *Advances in neural information processing systems*, 31, 2018.
- Pierre Comon. Independent component analysis, a new concept? *Signal processing*, 36(3):287–314, 1994.
- Aapo Hyvärinen and Erkki Oja. Independent component analysis: algorithms and applications. *Neural networks*, 13(4-5):411–430, 2000.
- Aleksandar Makelov, Georg Lange, and Neel Nanda. Is this the subspace you are looking for? an interpretability illusion for subspace activation patching. *arXiv preprint arXiv:2311.17030*, 2023.
- Mazda Moayeri, Keivan Rezaei, Maziar Sanjabi, and Soheil Feizi. Text-to-concept (and back) via cross-model alignment. In *International Conference on Machine Learning*, pages 25037–25060. PMLR, 2023.
- Mert Yuksekogunul, Maggie Wang, and James Zou. Post-hoc concept bottleneck models. *arXiv preprint arXiv:2205.15480*, 2022b.
- Tian Yun, Usha Bhalla, Ellie Pavlick, and Chen Sun. Do vision-language pretrained models learn composable primitive concepts? *arXiv preprint arXiv:2203.17271*, 2022.
- Chen Chen, Bowen Zhang, Liangliang Cao, Jiguang Shen, Tom Gunter, Albin Madappally Jose, Alexander Toshev, Jonathon Shlens, Ruoming Pang, and Yinfei Yang. Stair: Learning sparse text and image representation in grounded tokens. *arXiv preprint arXiv:2301.13081*, 2023.
- Yossi Gandelsman, Alexei A Efros, and Jacob Steinhardt. Interpreting clip’s image representation via text-based decomposition. *arXiv preprint arXiv:2310.05916*, 2023.
- Aditya Chattopadhyay, Ryan Pilgrim, and Rene Vidal. Information maximization perspective of orthogonal matching pursuit with applications to explainable ai. In *Thirty-seventh Conference on Neural Information Processing Systems*, 2023.
- Geoffrey Hinton. Taking inverse graphics seriously, 2013.
- Lukasz Romaszko, Christopher KI Williams, Pol Moreno, and Pushmeet Kohli. Vision-as-inverse-graphics: Obtaining a rich 3d explanation of a scene from a single image.

- In *Proceedings of the IEEE International Conference on Computer Vision Workshops*, pages 851–859, 2017.
- Vikram V Ramaswamy, Sunnie SY Kim, Ruth Fong, and Olga Russakovsky. Overlooked factors in concept-based explanations: Dataset choice, concept salience, and human capability. *arXiv preprint arXiv:2207.09615*, 2022.
- Christoph Schuhmann, Richard Vencu, Romain Beaumont, Robert Kaczmarczyk, Clayton Mullis, Aarush Katta, Theo Coombes, Jenia Jitsev, and Aran Komatsuzaki. Laion-400m: Open dataset of clip-filtered 400 million image-text pairs. *arXiv preprint arXiv:2111.02114*, 2021.
- Victor Weixin Liang, Yuhui Zhang, Yongchan Kwon, Serena Yeung, and James Y Zou. Mind the gap: Understanding the modality gap in multi-modal contrastive representation learning. *Advances in Neural Information Processing Systems*, 35:17612–17625, 2022.
- RZdunek ACichocki et al. Nonnegativematrixandtensor factorizations: Applicationstoexploratorymulti-waydata analysisandblindsourceseparation, 2009.
- Brian Murphy, Partha Talukdar, and Tom Mitchell. Learning effective and interpretable semantic models using non-negative sparse embedding. In *Proceedings of COLING 2012*, pages 1933–1950, 2012.
- Alona Fyshe, Partha P Talukdar, Brian Murphy, and Tom M Mitchell. Interpretable semantic vectors from a joint model of brain-and text-based meaning. In *Proceedings of the conference. Association for Computational Linguistics. Meeting*, volume 2014, page 489. NIH Public Access, 2014.
- Alona Fyshe, Leila Wehbe, Partha Talukdar, Brian Murphy, and Tom Mitchell. A compositional and interpretable semantic space. In *Proceedings of the 2015 conference of the north american chapter of the association for computational linguistics: Human language technologies*, pages 32–41, 2015.
- Zachary C. Lipton. The mythos of model interpretability, 2017.
- Marco Tulio Ribeiro, Sameer Singh, and Carlos Guestrin. ” why should i trust you?” explaining the predictions of any classifier. In *Proceedings of the 22nd ACM SIGKDD international conference on knowledge discovery and data mining*, pages 1135–1144, 2016.
- Gabriel Ilharco, Mitchell Wortsman, Ross Wightman, Cade Gordon, Nicholas Carlini, Rohan Taori, Achal Dave, Vaishal Shankar, Hongseok Namkoong, John Miller, Hannaneh Hajishirzi, Ali Farhadi, and Ludwig Schmidt. Openclip. July 2021. doi: 10.5281/zenodo.5143773. URL <https://doi.org/10.5281/zenodo.5143773>. If you use this software, please cite it as below.
- Alex Krizhevsky, Geoffrey Hinton, et al. Learning multiple layers of features from tiny images. 2009.
- Phillip Isola, Joseph J. Lim, and Edward H. Adelson. Discovering states and transformations in image collections. In *CVPR*, 2015.
- Ziwei Liu, Ping Luo, Xiaogang Wang, and Xiaoou Tang. Deep learning face attributes in the wild. In *Proceedings of International Conference on Computer Vision (ICCV)*, December 2015.
- Tsung-Yi Lin, Michael Maire, Serge Belongie, James Hays, Pietro Perona, Deva Ramanan, Piotr Dollár, and C Lawrence Zitnick. Microsoft coco: Common objects in context. In *Computer Vision—ECCV 2014: 13th European Conference, Zurich, Switzerland, September 6-12, 2014, Proceedings, Part V 13*, pages 740–755. Springer, 2014.
- J. Deng, W. Dong, R. Socher, L.-J. Li, K. Li, and L. Fei-Fei. ImageNet: A Large-Scale Hierarchical Image Database. In *CVPR09*, 2009.
- F. Pedregosa, G. Varoquaux, A. Gramfort, V. Michel, B. Thirion, O. Grisel, M. Blondel, P. Prettenhofer, R. Weiss, V. Dubourg, J. Vanderplas, A. Passos, D. Cournapeau, M. Brucher, M. Perrot, and E. Duchesnay. Scikit-learn: Machine learning in Python. *Journal of Machine Learning Research*, 12:2825–2830, 2011.
- Amir Beck and Marc Teboulle. A fast iterative shrinkage-thresholding algorithm for linear inverse problems. *SIAM journal on imaging sciences*, 2(1):183–202, 2009.
- Stephen Boyd, Neal Parikh, Eric Chu, Borja Peleato, Jonathan Eckstein, et al. Distributed optimization and statistical learning via the alternating direction method of multipliers. *Foundations and Trends® in Machine learning*, 3(1):1–122, 2011.

A Relationship between cosine similarity and MSE optimization.

Recall our ℓ_1 relaxed cosine similarity optimization problem from Eqn. (1),

$$\min_{\mathbf{w} \in \mathbb{R}_+^c} \|\mathbf{w}\|_0 \quad \text{s.t.} \quad \langle \mathbf{z}, \frac{\mathbf{C}\mathbf{w}}{\|\mathbf{C}\mathbf{w}\|_2} \rangle \geq 1 - \epsilon. \quad (4)$$

First we relax the ℓ_0 constraint to an ℓ_1 penalty.

$$\max_{\mathbf{w} \in \mathbb{R}_+^c} \langle \mathbf{z}, \frac{\mathbf{C}\mathbf{w}}{\|\mathbf{C}\mathbf{w}\|_2} \rangle - \lambda \|\mathbf{w}\|_1. \quad (5)$$

By observing that $\|x - y\|_2^2 = \langle x - y, x - y \rangle = \langle x, x \rangle + \langle y, y \rangle - 2\langle x, y \rangle$ and that $\mathbf{z}, \frac{\mathbf{C}\mathbf{w}}{\|\mathbf{C}\mathbf{w}\|_2}$ are unit-norm, maximizing the above inner product is equivalent to minimizing the euclidean norm,

$$\min_{\mathbf{w} \in \mathbb{R}_+^c} \left\| \frac{\mathbf{C}\mathbf{w}}{\|\mathbf{C}\mathbf{w}\|_2} - \mathbf{z} \right\|_2^2 + 2\lambda \|\mathbf{w}\|_1. \quad (6)$$

This is a non-convex problem, but we can relax this problem to achieve better reconstruction in terms of euclidean distance as shown in Eqn. (2),

$$\min_{\mathbf{w} \in \mathbb{R}_+^c} \|\mathbf{C}\mathbf{w} - \mathbf{z}\|_2^2 + 2\lambda \|\mathbf{w}\|_1. \quad (7)$$

This problem will optimize euclidean distance between $\mathbf{C}\mathbf{w}$ and \mathbf{z} . Consider two vectors x, y on the unit sphere such that $\langle \frac{x}{\|x\|}, \frac{y}{\|y\|} \rangle > 0$. While any vector αy , $\alpha > 0$ will have the same cosine similarity score, the optimal vector in terms of euclidean distance to x is the vector αy such that $\alpha = \text{proj}_y(x)$, or in other words the projection of x onto y . Thus, solving for euclidean distance to approximate x will find αy which we must then normalize to find the unit-norm solution y . This explains the normalizing process described in Section 4.2.

Additionally, we can view Eqn. (7) as applying shrinkage to $\mathbf{C}\mathbf{w}$. Reverting from euclidean norm to inner product, Eqn. (7) becomes

$$\max_{\mathbf{w} \in \mathbb{R}_+^c} \langle \mathbf{C}\mathbf{w}, \mathbf{z} \rangle - \frac{1}{2} \langle \mathbf{C}\mathbf{w}, \mathbf{C}\mathbf{w} \rangle - \lambda \|\mathbf{w}\|_1 = \langle \mathbf{C}\mathbf{w}, \mathbf{z} \rangle - \frac{1}{2} \|\mathbf{C}\mathbf{w}\|_2^2 - \lambda \|\mathbf{w}\|_1. \quad (8)$$

In conclusion, our optimization problem maximizes the inner product while imposing a shrinkage penalty and sparsity penalty. Empirically, our reconstructions $\mathbf{C}\mathbf{w}$ are low-norm, so we normalize after solving to recover the unit-norm reconstruction.

B ADMM for batched on-device LASSO optimization.

As each decomposition requires solving a LASSO optimization problem, we implement the Alternating Direction Method of Multipliers (ADMM) algorithm in Pytorch over batches with GPU support for efficient decomposition of large scale datasets over large numbers of concepts Boyd et al. [2011]. In practice, ADMM achieves primal and dual tolerances of $1e - 4$ in fewer than 1000 iterations on a batch size of 1024.

Next we derive the iterates for our ADMM algorithm. Recall our optimization problem,

$$\min_{\mathbf{w} \in \mathbb{R}_+^c} \|\mathbf{C}\mathbf{w} - \mathbf{z}\|_2^2 + 2\lambda \|\mathbf{w}\|_1. \quad (9)$$

ADMM breaks down convex optimization problems into multiple sub-problems while penalizing the difference in solutions. We break Eqn. (9) into two subproblems, one solving the euclidean distance objective and one solving the ℓ_1 and nonnegativity constraint. We let w denote the former solution, z the latter, and u tracks the difference between the two. Our ADMM iterates (w^k, z^k, u^k) are

$$w^{k+1} = \arg \min_w (f(w) + \frac{\rho}{2} \|w^k - z^k + u^k\|_2^2), \quad (10)$$

$$z^{k+1} = (S_{\lambda/\rho}(w^{k+1} + u^k))_+, \quad (11)$$

$$u^{k+1} = u^k + w^{k+1} - z^{k+1}, \quad (12)$$

where S_κ is a soft-thresholding function used to satisfy the LASSO constraints,

$$S_\kappa(a) := \begin{cases} a - \kappa, & a > \kappa \\ 0, & |a| \leq \kappa \\ a + \kappa, & a < -\kappa \end{cases} \quad (13)$$

As our optimization function $f(w)$ is quadratic, we can analytically compute w^{k+1} as

$$w^{k+1} = (2C^T C + \rho)^{-1}(\rho v + 2Cw), \quad (14)$$

where $v = z^k - u^k$. In our experiments we set $\rho = 5$, and stop when tolerances $\epsilon_{\text{prim}} = \|x^{k+1} - z^{k+1}\|_2$, $\epsilon_{\text{dual}} = \|\rho(z^{k+1} - z^k)\|_2$ are less than $1e - 4$. Over a batch, we iterate until every solver in the batch has reached the above tolerances.

C When do Sparse Decompositions Exist?

Theorem C.1. *Given Assumptions 4.1 - 4.4, CLIP image embeddings f can be written as a sparse linear combination of text embeddings, i.e.,*

$$f(\mathbf{x}^{\text{img}}) = \mathbf{C}^{\text{txt}} \mathbf{w}; \quad \text{s.t.} \quad \|\mathbf{w}\|_0 \leq \alpha$$

where $\mathbf{w} \in \mathbb{R}_+^k$, and $\mathbf{C}^{\text{txt}} \in \mathbb{R}^{d \times k}$, which is the text concept dictionary defined previously.

Proof. Any vector ω can be written as $\omega = \sum_{i=1}^k \omega_i \mathbf{e}_i$, where $\omega_i \in \mathbb{R}_+$, and $\mathbf{e}_i \in \mathbb{R}^k$ is a one-hot vector with one at the i^{th} co-ordinate. Thus we have

$$f(\mathbf{x}^{\text{img}}) = f \circ h^{\text{img}}(\omega, \epsilon) = f \circ h^{\text{img}}(\omega) = f \circ h^{\text{img}}\left(\sum_{i=1}^k \omega_i \mathbf{e}_i\right) = \sum_{i=1}^k \omega_i \underbrace{f \circ h^{\text{img}}(\mathbf{e}_i)}_{\mathbf{c}_i^{\text{img}}} \quad (\text{Assumption 4.2})$$

Here we define $\mathbf{c}_i^{\text{img}} = f \circ h^{\text{img}}(\mathbf{e}_i)$ as the ‘image’ concept basis vector; analogous to the text concept basis vector $\mathbf{c}_i^{\text{txt}} = g \circ h^{\text{txt}}(\mathbf{e}_i)$ already defined. Thus Assumption 4.2 implies the existence of a sparse decomposition of f in terms of ‘image’ concept vectors $\mathbf{c}_i^{\text{img}}$. Additionally, Assumption 4.1 ensures that this decomposition is sparse, as ω is sparse. So far, we have $f(\mathbf{x}^{\text{img}}) = \mathbf{C}^{\text{img}} \omega$ s.t. $\|\omega\|_0 \leq \alpha$.

From Assumption 4.3, the image concept vectors and text concept vectors are equal to each other, i.e., $\mathbf{c}_i^{\text{img}} = f \circ h^{\text{img}}(\mathbf{e}_i) = g \circ h^{\text{txt}}(\mathbf{e}_i) = \mathbf{c}_i^{\text{txt}}$. Finally, from Assumption 4.4, we have that the text concept vectors $\mathbf{c}_i^{\text{txt}}$ are given simply by word embeddings g of individual words.

Stringing these arguments together, we have that image representations $f(\mathbf{x}^{\text{img}})$ can be written as a sparse linear combination of vectors obtain from CLIP word embeddings $\mathbf{c}_i^{\text{txt}}$. We finally set $\mathbf{w} = \omega$, thus proving the assertion. \square

D Additional ImageNet Concept Histograms

We present concept histograms for the top seven concepts of five more ImageNet classes: {‘Face Powder’, ‘Feather Boa’, ‘Jack-O’-Lantern’, ‘Kimono’, ‘Dalmation’}, similar to Figure 6. These decompositions give insights both into the distribution of each class as well as some biases of CLIP. For example, the concepts “kitten” and “chihuahua” are present in the ‘Feather Boa’ decomposition, and were confirmed via manual inspection where we found 2 images of chihuahuas and 3 images of cats wearing boas in the dataset. For ‘Face Powder’, the concept “benefit” is the third most common concept, and it is indeed a common cosmetic brand name in the images. For the ‘Dalmation’ class, we see that the decompositions consists of concepts relating to dogs and black and white spots, which together make up the high-level concept of a dalmation. Finally, for the class ‘Kimono’, the concepts “doll”/“dolls” are the third and fourth most common, although all of the images in the ‘Kimono’ class were of real humans, not of dolls. This highlights an implicit bias in CLIP’s representations or in the descriptions of people wearing kimonos in CLIP’s training set.

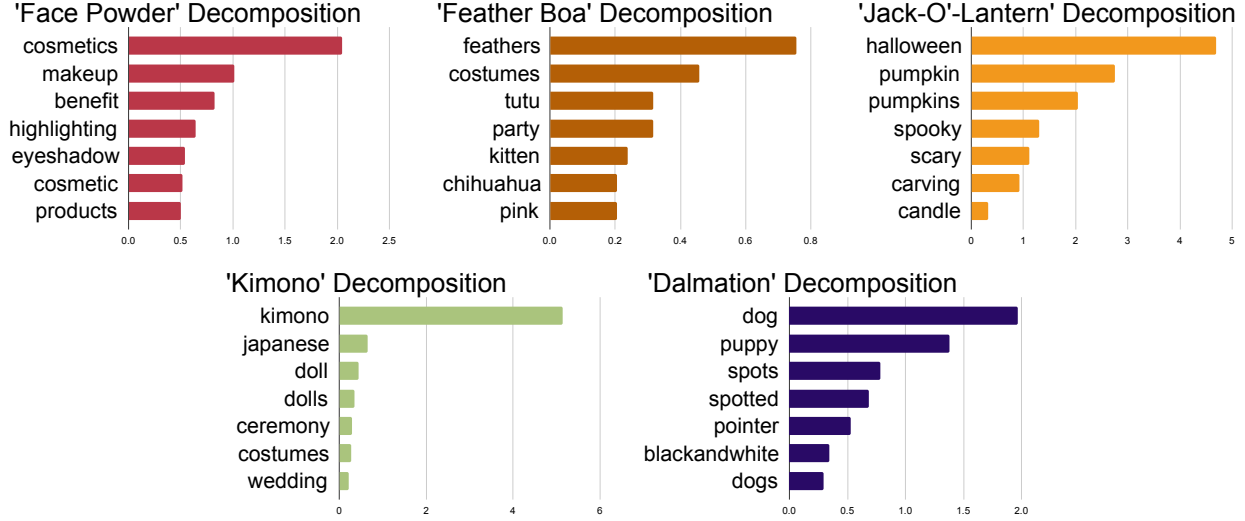


Figure 9: Example concept histograms of various ImageNet classes. The top seven concepts for each class are visualized along with their relative weighting, with the average ℓ_0 norm of individual sample decompositions also being 7.

Table 2: Linearity of CLIP Embeddings.

	w_a	w_b	$\text{COSINE}(\hat{z}, z)$
IMAGENET	0.48 ± 0.09	0.45 ± 0.09	0.76 ± 0.05
CIFAR100	0.45 ± 0.08	0.42 ± 0.08	0.75 ± 0.03
MIT STATES	0.48 ± 0.09	0.45 ± 0.09	0.76 ± 0.05
COCO TEXT	0.59 ± 0.12	0.47 ± 0.12	0.88 ± 0.04

E Additional Experiments

In this section we present additional experiments including (1) sanity checking the linearity of dense CLIP embeddings, (2) ablation studies on the mean centering operation, choice of concept vocabulary, and distribution of types of concepts highlighted by SpLiCE, (3) SpLiCE performance on probing tasks, (4) additional results for SpLiCE’s performance on retrieval tasks, and (5) experiments on an alternative CLIP model from OpenAI with a ResNet50 visual backbone.

E.1 Sanity Checking CLIP’s Linearity

We begin by asking the following question to confirm the general linearity of CLIP embeddings: “if two inputs are concatenated, does their joint embedding equal the average of their two individual embeddings?”. For the image domain, we combine two images, x_a, x_b , to form their composition x_{ab} by placing x_a in the top left quarter and x_b in the bottom right quarter of a blank image. For the text domain, we simply append text x_b to text x_a to form x_{ab} . We then embed x_a, x_b, x_{ab} with CLIP to get z_a, z_b, z_{ab} . Solving the equation $w_a * z_a + w_b * z_b = z_{ab}$ for scalar weights w_a, w_b then allows us to assess the linearity of z_a, z_b, z_{ab} . We report w_a, w_b and the cosine similarity between $\hat{z}_{ab} = [z_a, z_b] \cdot [w_a, w_b]$ and z_{ab} in Table 2.

In general, we find that the composition of two inputs results in an embedding that is approximately equal to the average of the two input components, with w_a, w_b being very close to 0.5 across all datasets and for both modalities.

E.2 Ablation Studies

Mean Centering. In order to empirically check that the mean centering of images does not result in a loss of information, we decompose the img mean, μ_{img} , that we used for all experiments. If we decompose it with uncentered concepts, the following concepts are highlighted: {“posed”, “added”, “pics”, “artist”, “caption”}. The decomposition with centered

concepts results in the following concepts: {“closeup”, “posed”, “flicker”}. These concepts all seem to be generally related to images, with minimal other semantic information, suggesting that centering does not remove any discriminative semantic content of embeddings, but simply removes information about the modality.

Choice of Concept Vocabulary. We perform a simple ablation study to assess the sensitivity of our method to choices in concept vocabulary. We collect a second vocabulary in the same exact manner as the LAION vocabulary from the MSCOCO caption dataset. We consider both the top 10k and top 5k most common words for both, and repeat the zero-shot accuracy and reconstruction cosine similarity experiments from Section 5.2 on CIFAR100. We see that the MSCOCO10k and LAION10k vocabularies perform almost exactly the same for both metrics. The smaller vocabularies perform the same for cosine reconstruction but underperform the 10k vocabularies for zero-shot classification tasks.

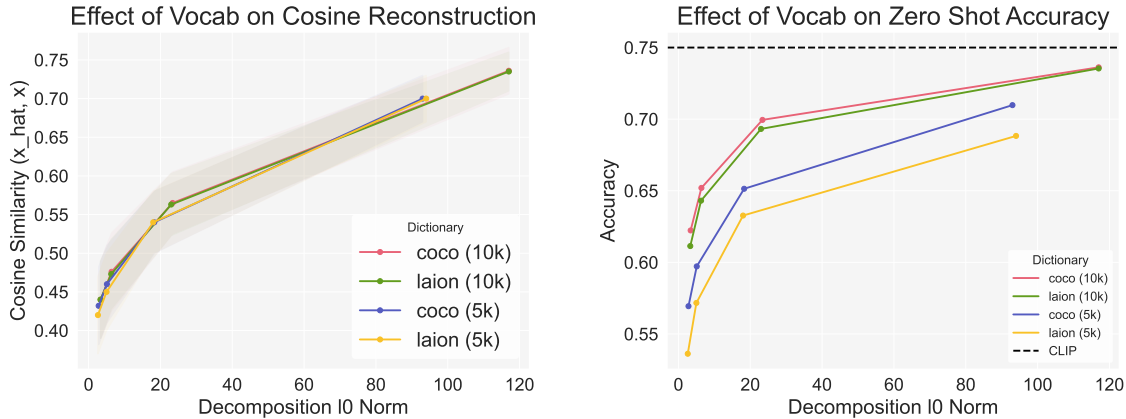


Figure 10: Change in SpLiCE performance when considering another semantic concept dictionary derived from MSCOCO as well as a smaller concept vocabulary.

Concept Type Distribution. In order to better understand any biases produced by the decomposition process or that CLIP itself has, we visualize the types of concepts most commonly activated across multiple datasets, labelling them by part of speech in Figure 11. We see that nouns are by far the most common concepts across datasets, indicating that both CLIP and the decompositions are highly object centric. Note that the low weight on verbs and adjective is due to far fewer concepts of those types being activated (low l_0 norm) as well as the weight upon those concepts being significantly smaller (low l_1 norm). We hypothesize that the information in many adjective and verbs can actually be encoded into the noun itself, resulting in this phenomenon. For example, the concept “lemon” is a more succinct form of “yellow” and “fruit”.

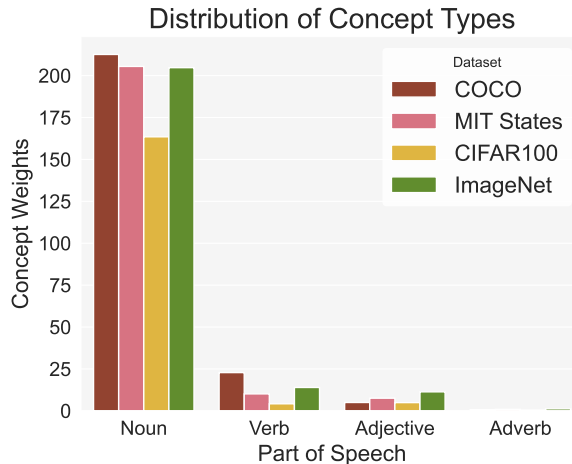


Figure 11: SpLiCE decompositions are mostly comprised of nouns across multiple datasets.

E.3 Performance of SpLiCE on Probing Tasks

We evaluate the performance of the decompositions on probes trained on both regular CLIP embeddings as well as decomposed CLIP embeddings for CIFAR100 in 3 and MIT States in 4. We consider two scenarios: a probe trained on CLIP embeddings and tested on SpLiCE embeddings of various sparsities (shown in row CLIP PROBE), and a probe both trained and evaluated on SpLiCE embeddings (shown in row SpLiCE PROBE). We report mean over three runs, with standard deviations for each experiment being less than 0.005. We find that SpLiCE representations closely match the performance of dense CLIP embeddings, with a slight drop in performance when probes are trained directly on SpLiCE embeddings rather than trained on CLIP embeddings and evaluated on SpLiCE embeddings for CIFAR100.

Table 3: Evaluation of Probing Performance on CIFAR100

	$l_0 = 3$	$l_0 = 6$	$l_0 = 23$	$l_0 = 117$	CLIP
SPLiCE PROBE	0.95	0.95	0.95	0.95	–
CLIP PROBE	0.96	0.96	0.97	0.97	0.97

Table 4: Evaluation of Probing Performance on MIT States

	$l_0 = 4$	$l_0 = 7$	$l_0 = 27$	CLIP
SPLiCE PROBE	0.883	0.883	0.882	–
CLIP PROBE	0.883	0.883	0.884	0.883

E.4 Additional Retrieval Experiments

We present additional results for the performance of SpLiCE embeddings on text-to-image and image-to-text retrieval tasks. We evaluate retrieval over various 1024 sample sub-sets of MSCOCO, and assess recall performance for the top-k closest embeddings of the opposite modality. We visualize $k = \{1, 10\}$ in Figure 12 and $k = \{5\}$ in Figure 5. We find that our semantic concept dictionaries outperform all baselines when decomposition sparsity is high, but that dictionaries learned over images perform best for text to image retrieval when decompositions have greater than 30 nonzero concepts.

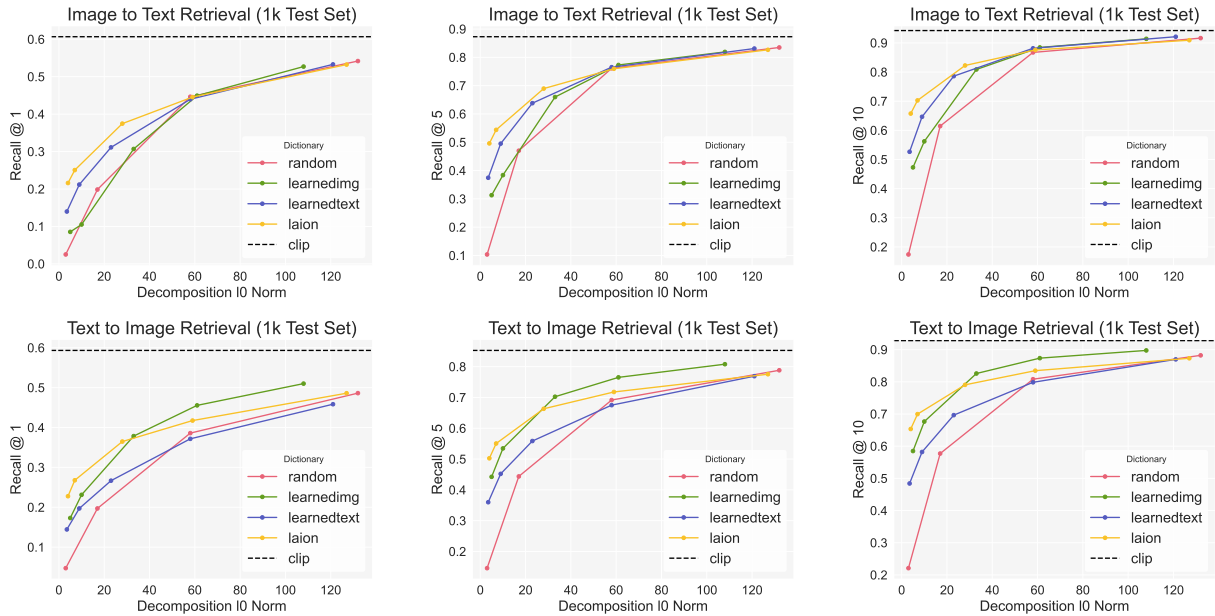


Figure 12: Top-1 , 5, 10 performance of SpLiCE representations on image-to-text (top) and text-to-image (bottom) retrieval on MSCOCO.

E.5 Experiments on Alternative CLIP Architecture

We present experiments with an alternative CLIP architecture from OpenAI with a ResNet50 backbone for the vision encoder. We find that results are similar to those presented in 4, save for OpenAI’s ResNet50 CLIP performing much worse than OpenCLIP’s ViT B/32 backbone in general.



Figure 13: Performance of SpLiCE decomposition representations on zero-shot classification tasks (bottom row) and cosine similarity between CLIP embeddings and SpLiCE embeddings (top row) for OpenAI’s ResNet50 CLIP model.